Journal of the American College of Cardiology
© 2013 by the American College of Cardiology Foundation
Published by Elsevier Inc.

Vol. 61, No. 22, 2013
ISSN 0735-1097/$36.00
http://dx.doi.org/10.1016/j.jacc.2012.11.083

STATE-OF-THE-ART PAPER

Computational Fluid Dynamics Applied to Cardiac Computed Tomography for Noninvasive Quantification of Fractional Flow Reserve

Scientific Basis

Charles A. Taylor, PhD,*† Timothy A. Fonte, BS,* James K. Min, MD‡

Redwood City, Stanford, and Los Angeles, California

Coronary computed tomography angiography (CTA) has emerged as a noninvasive method for direct visualization of coronary artery disease, with previous studies demonstrating high diagnostic performance of CTA compared with invasive coronary angiography. However, CTA assessment of coronary stenoses tends toward overestimation, and even among CTA-identified severe stenosis confirmed at the time of invasive coronary angiography, only a minority are found to be ischemia causing. Recent advances in computational fluid dynamics and image-based modeling now permit determination of rest and hyperemic coronary flow and pressure from CTA scans, without the need for additional imaging, modification of acquisition protocols, or administration of medications. These techniques have been used to noninvasively compute fractional flow reserve (FFR), which is the ratio of maximal coronary blood flow through a stenotic artery to the blood flow in the hypothetical case that the artery was normal, using CTA images. In the recently reported prospective multicenter DISCOVER-FLOW (Diagnosis of Ischemia-Causing Stenoses Obtained Via Noninvasive Fractional Flow Reserve) study and the DeFACTO (Determination of Fractional Flow Reserve by Anatomic Computed Tomographic Angiography) trial, FFR derived from CTA was demonstrated as superior to measures of CTA stenosis severity for determination of lesion-specific ischemia. Given the significant interest in this novel method for determining the physiological significance of coronary artery disease, we herein present a review on the scientific principles that underlie this technology. (J Am Coll Cardiol 2013;61:2233–41) © 2013 by the American College of Cardiology Foundation

Coronary revascularization is often performed on an ad hoc basis from semiquantitative measures of percent luminal diameter narrowing of the artery visualized at the time of invasive coronary angiography (ICA) (1). This practice stems from the research of Gould et al. (2), who elegantly demonstrated the relationship between stenosis and ischemia, as determined by myocardial blood flow reserve, wherein flow to the myocardium is compromised as the luminal diameter progressively narrows. This diminution in flow is most evident at hyperemic states and begins as early as 40% narrowing of vessel diameter, with more predictable reductions in hyperemic flow for stenoses ≥70% (3).

However, the relationship between coronary stenosis and myocardial ischemia is more complex, with ensuing studies demonstrating an unreliable relationship between stenosis and ischemia (4). One example of this was highlighted in the nuclear substudy of the COURAGE (Clinical Outcomes Utilizing Revascularization and Aggressive Drug Evaluation) trial; in this study in patients with ≥70% stenosis, only 32% exhibited severe ischemia and 40% manifested no or mild ischemia according to myocardial perfusion scintigraphy (5).

At present, the gold standard assessment of the hemodynamic significance of coronary stenoses is fractional flow reserve (FFR) (6). FFR uses a pressure wire to determine the ratio of maximal coronary blood flow through a stenotic artery to the blood flow in the hypothetical case that the artery was normal, and it is the only diagnostic method to date for ischemia detection to demonstrably advance event-free survival (7,8). In the FAME (Fractional Flow Reserve Versus Angiography for Multivessel Evaluation) trial of 1,005 patients with multivessel coronary artery disease (CAD), FFR-guided revascularization (i.e, revascularization for lesions with FFR ≤0.80) was associated with a 28% lower rate of major adverse cardiac events compared with an angiography-guided strategy. The salutary outcomes for individuals undergoing FFR-guided revascularization are long-lived and cost-saving (9). The results from FAME are

From *HeartFlow, Inc., Redwood City, California; †Department of Bioengineering, Stanford University, Stanford, California; and the ‡Cedars-Sinai Heart Institute, Los Angeles, California. Dr. Taylor and Mr. Fonte are employees and shareholders of HeartFlow, Inc., which provides the FFR_{CTA} service. Dr. Min is a member of the Speaker's Bureau and medical advisory board of General Electric; and has an equity interest in TC3.

Manuscript received June 15, 2012; revised manuscript received October 19, 2012, accepted November 20, 2012.

Abbreviations and Acronyms

CAD = coronary artery disease
CFD = computational flow dynamics
CFR = coronary flow reserve
CT = computed tomography
FFR = fractional flow reserve
ICA = invasive coronary angiography
LAD = left anterior descending
LCx = left circumflex
MACE = major adverse cardiac event(s)
MBF = myocardial blood flow
MPS = myocardial perfusion scintigraphy
NPV = negative predictive value
PPV = positive predictive value
RCA = right coronary artery

in accordance with the 5-year follow-up of individuals from the DEFER (Deferral Versus Performance of PTCA in Patients Without Documented Ischemia) study (7). Among lesions judged angiographically "obstructive," >50% were hemodynamically insignificant according to FFR. No benefit was observed for revascularization in patients with hemodynamically insignificant lesions. In the FAME 2 trial, FFR-guided therapy reduced the need for urgent revascularization in patients with stable CAD and hemodynamically significant lesions (10).

Coronary computed tomography angiography (CTA) is a noninvasive method for visualization of CAD (11–13). Previous CTA studies have observed an overestimation of stenosis severity, and even among high-grade stenoses according to CTA confirmed by using ICA, only a minority cause ischemia (14,15). Coronary lesions considered severe according to CTA cause ischemia less than one-half of the time (15). These findings have provoked concerns that widespread application of CTA may encourage unnecessary ICA (16).

Numerous imaging tests exist for physiological assessment of CAD, including stress echocardiography, cardiac magnetic resonance, and myocardial perfusion scintigraphy. These modalities assess wall motion abnormalities or regional differences in coronary flow reserve (CFR) as a surrogate for ischemia and identify individuals who may have severe stenoses. Although robust for ischemia detection on a per-patient basis, these tests demonstrate poor discrimination of specific vessels with coronary lesions that cause ischemia. As an example, when using an FFR standard for vessel-specific ischemia, myocardial perfusion scintigraphy identifies ischemic territories correctly <50% of the time, with underestimation and overestimation in 36% and 22% of cases, respectively (17). Such data have evoked concerns for the ability of stress testing to effectively isolate coronary lesions that benefit from revascularization.

Recent advances in computational fluid dynamics enable calculation of coronary flow and pressure fields from anatomic image data (18). Applied to CTA, these technologies enable calculation of FFR without additional imaging or medications. The DISCOVER-FLOW (Diagnosis of Ischemia-Causing Stenoses Obtained Via Noninvasive Fractional Flow Reserve) trial, compared with invasive FFR, noninvasive FFR derived from CTA, or FFR_{CTA}, demonstrated per-vessel accuracy, sensitivity, specificity, positive predictive value (PPV), and negative predictive value (NPV) for lesions causing ischemia of 84.3%, 87.9%, 82.2%, 73.9%, and 92.2%, respectively, for FFR_{CTA} (19). The performance of FFR_{CTA} was superior to CTA stenosis for diagnosing ischemic lesions, the latter of which demonstrated an accuracy, sensitivity, specificity, PPV, and NPV of 58.5%, 91.4%, 39.6%, 46.5%, and 88.9%, respectively. Case examples of non–ischemia-causing and ischemia-causing stenoses can be seen in Figures 1 and 2, respectively. More recently, the DeFACTO (Determination of Fractional Flow Reserve by Anatomic Computed Tomographic Angiography) trial, a pivotal multicenter international study evaluating FFR_{CTA} against CTA for diagnostic accuracy of ischemia, has been published (20). This trial consisted of 252 patients for which 407 vessels were directly interrogated by using FFR. On a per-patient basis, FFR_{CTA} was superior to CTA stenosis for diagnosis of ischemic lesions for accuracy (73% vs. 64%), sensitivity (90% vs. 84%), specificity (54% vs. 42%), PPV (67% vs. 61%), and NPV (84% vs. 72%). In patients with intermediate stenoses (30% to 70%), there was a more than 2-fold increase in sensitivity, from 37% to 82%, with no loss of specificity.

Given the rapid clinical evidence development of FFR_{CTA}, we herein present the fundamental tenets that underlie the basis of computational modeling of coronary flow and pressure.

Cardiovascular Form and Function Relationships

Computation of FFR_{CTA} requires construction of an anatomic model of the coronary arteries; a mathematical model of coronary physiology to derive boundary conditions representing cardiac output, aortic pressure, and microcirculatory resistance; and a numerical solution of the laws of physics governing fluid dynamics. This combination of anatomy, physiology, and fluid dynamics enables the computation of coronary flow and pressure.

Anatomic data obtained from CTA contains a wealth of information on coronary blood flow because "form follows function" in circulatory systems (21). These form–function relationships are universal and enable the circulation to provide an adequate supply of blood at appropriate pressures to organs under varying physiological states (e.g., exercise) and to adapt to chronic changes, including disease progression. Allometric scaling laws, which relate the mass of an object to shape, anatomy, and physiology, are critical for defining cardiovascular form–function relationships and are broadly applicable to the entire cardiovascular system (22). Allometric scaling laws also enable relation of organ size to flow rate. For example, under resting conditions, total coronary flow is proportional to myocardial mass, $Q_c \propto M_{myo}^{\beta}$ (23). Mass can be calculated from myocardial volume, which is easily extracted from volumetric CTA data.

Form–function relationships also apply directly to coronary arteries, which may dilate or constrict to modulate organ blood flow (e.g., in exercise), enlarge in response to chronic

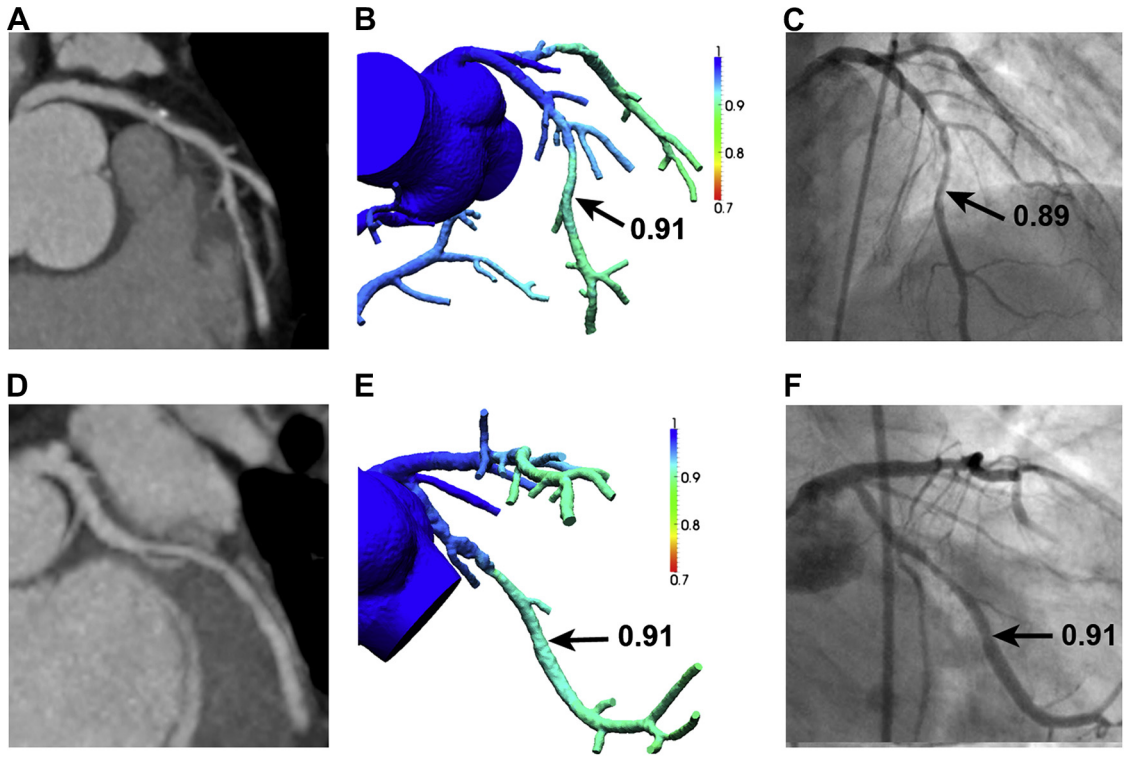

Figure 1 **FFR_{CTA} Results for 66-Year-Old Man With Multivessel CAD But No Lesion-Specific Ischemia**

(A) Coronary computed tomography angiography (CTA) demonstrating stenosis in the left anterior descending coronary artery (LAD). **(B)** Fractional flow reserve (FFR) derived from CTA (FFR_{CTA}) demonstrates no ischemia in the LAD, with a computed value of 0.91. **(C)** Invasive coronary angiography (ICA) with FFR also demonstrates no ischemia in the LAD, with a measured value of 0.89. **(D)** CTA demonstrating stenosis in the left circumflex coronary (LCx) artery. **(E)** FFR_{CTA} demonstrates no ischemia in the LCx, with a computed value of 0.91. **(F)** ICA with FFR also demonstrates no ischemia in the LCx, with a measured value of 0.91.

increases in blood flow (e.g., in arteriovenous fistulas), or diminish in caliber in response to reductions in blood flow. The mathematical relationship between vessel size and flow rate was first proposed by Murray (24) in 1926, as $Q \propto d^k$, where Q is the flow rate through a blood vessel, d is its diameter, and k is a constant derived empirically for which Murray proposed a value of 3. In its simplest form, Murray's law is the manifestation of adaptive mechanisms whereby blood vessels sense the level of shear stress on the endothelial surface and remodel to maintain homeostasis. This flow–diameter relationship can be understood by considering Poiseuille's solution, which relates vessel flow rate, Q, vessel diameter, d, and the wall shear stress, τ_w, by the formula:

$$Q = \frac{\pi}{32\mu}\tau_w d^3 \qquad \text{[Equation 1]}$$

where μ is the fluid viscosity. If wall shear stress is maintained at a constant, homeostatic level, then this formula implies that $Q \propto d^3$, and Murray's law is recovered. Empirically, blood vessels have been proven to modulate their size based on the flow they carry and the wall shear stress sensed by the endothelial cells (25). These adaptive processes typically complete in a few weeks (4 to 6 weeks) (26) and continue even in the presence of atherosclerosis (27). Consequently, a coronary vessel that subtends a myocardial territory with lower perfusion will diminish in caliber, whereas chronic increases in blood flow, as might be observed subsequent to revascularization of a coronary stenosis or after initiation of an exercise regimen, will result in luminal enlargement.

Morphometry laws of the form $Q \propto d^k$ provide additional physiological information for assessing the relative resistance to flow of branches arising from the coronary arteries. Under resting conditions, the mean pressure, p, down the length of a coronary artery is largely constant and forces flow through each branch in accordance with the relationship:

$$p = QR \qquad \text{[Equation 2]}$$

where R is the resistance to flow of the branch vessel. Therefore, $Q \propto d^k$ implies that $R \propto d^{-k}$, or that the resistance to flow of each branch is inversely related to vessel size, with the same morphometric exponent, k, relating flow to diameter. Thus, small coronary branches have a higher resistance to flow than larger branches, and the resistance to

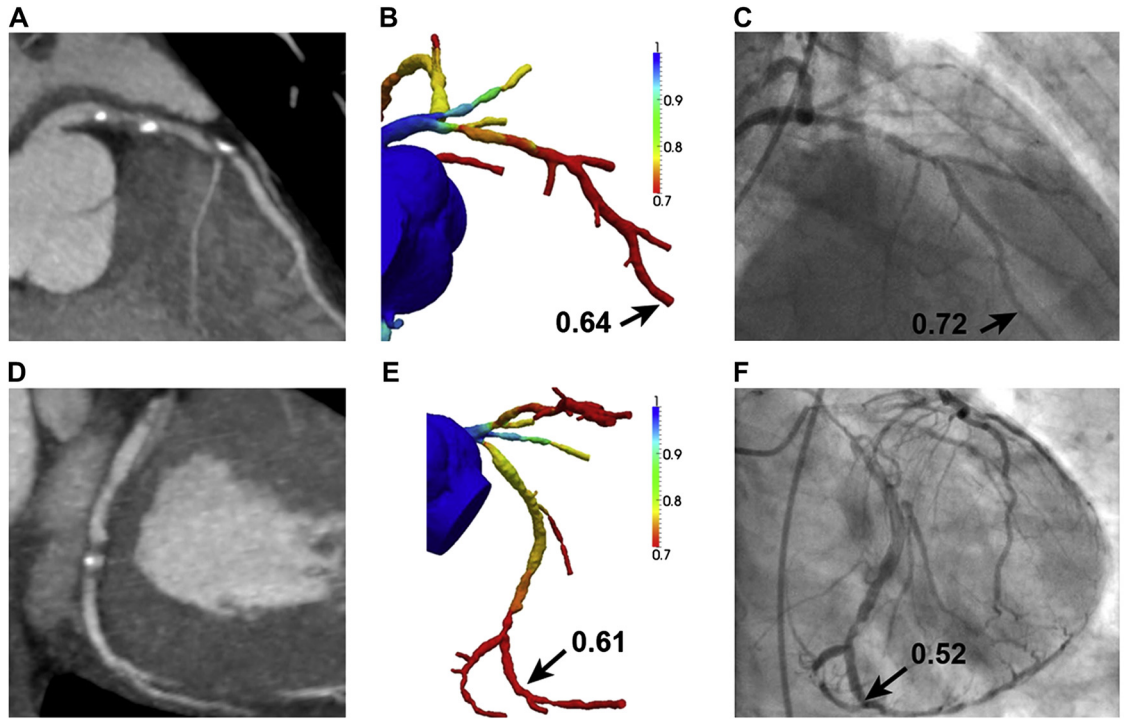

Figure 2 **FFR_{CTA} Results for 66-Year-Old Man With Multivessel CAD and Lesion-Specific Ischemia**

(A) CTA demonstrating stenosis in the LAD. **(B)** FFR_{CTA} demonstrates ischemia in the LAD, with a computed value of 0.64. **(C)** ICA with FFR also demonstrates ischemia in the LAD, with a measured value of 0.72. **(D)** CTA demonstrating stenosis in the LCx. **(E)** FFR_{CTA} demonstrates ischemia in the LCx, with a computed value of 0.61. **(F)** ICA with FFR also demonstrates ischemia in the LCx, with a measured value of 0.52. Abbreviations as in Figure 1.

flow distal to a stenosis will be directly related to the number and size of vessels downstream.

Computational Fluid Dynamics

Coronary flow and pressure can be computed by solving the governing equations of fluid dynamics, which relate to conservation of mass and balance of momentum, and which have been known in their current forms as the Navier-Stokes equations for >150 years. These equations are solved for the unknown pressure, which varies with position and time, and for the 3 components of blood velocity, each of which are functions of position and time. The physical properties of blood, the fluid density and the fluid viscosity, are known when solving these equations. Although blood exhibits complex rheological properties, it can be approximated as a Newtonian fluid with a constant viscosity in large arteries.

Notable features of the equations of fluid dynamics are their universality for describing phenomena ranging from airflow over a jetliner to water flow in a river to blood flow in arteries, as well as their ability to capture complex phenomena. However, the governing equations of blood flow can only be solved analytically under special circumstances (e.g., steady or pulsatile flow in an idealized circular cylindrical geometry). For realistic patient-specific models of the human coronary arteries, a numerical method must instead be used to approximate the governing equations and to obtain a solution for velocity and pressure at a finite number of points (28). This requires solving millions of nonlinear partial differential equations simultaneously and repeating this process for thousands of time intervals in a cardiac cycle. Numerical methods for solving fluid dynamics problems are known as computational fluid dynamics (CFD) methods.

The governing equations are insufficient to solve blood flow problems; a domain of interest must be defined, and boundary conditions need to be specified. Boundary conditions are mathematical relationships between the variables of interest (e.g., flow and pressure) defined on the boundaries of the mathematical model. Specific to modeling blood flow in arteries, the domain of interest is where the blood is flowing (i.e., the lumen), and the relevant boundaries are the lateral surface, the inlet boundary (the aortic root), and the outlet boundaries of the ascending aorta and the coronary arteries.

It is virtually impossible to directly represent the heart and the >5 billion blood vessels in the human circulation, so the domain of interest for CFD models of arterial blood flow is a defined portion of the vascular system. Consequently, it is necessary to describe the conditions at the interface of the modeled domain and the remainder of the

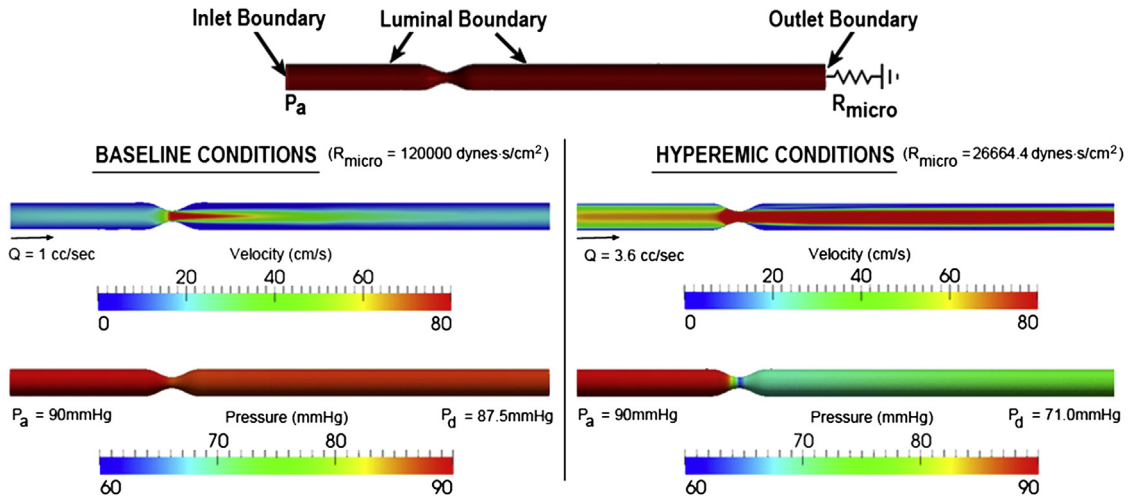

Figure 3 **Mathematical Model of Blood Flow Through an Idealized LAD Stenosis With a Reference Diameter of 3.5 mm and a 60% Diameter Reduction Stenosis**

A constant pressure (P_a = 90 mm Hg) is applied at the inlet boundary, and a constant resistance, R_{micro}, is prescribed at the outlet boundary to simulate the downstream microcirculatory resistance. The velocity is set at zero along the luminal boundary. R_{micro} is set at 120,000 dynes·s/cm^2 to model baseline conditions with a flow rate of 1 cc/s and is reduced by a factor of 4.5 to 26,664.4 dynes·s/cm^2 to model hyperemic conditions. Hyperemic flow increases to 3.6 cc/s. The velocity on a slice along the vessel illustrates that a jet through the stenosis rapidly dissipates under baseline conditions but persists under hyperemic conditions. (P_d/P_a = 0.97 at baseline, FFR = P_d/P_a = 0.79 at hyperemia). Abbreviations as in Figure 1.

circulation. Figure 3 illustrates these concepts in an idealized model of steady flow through a single coronary artery with a stenosis.

Image-Based Modeling of Blood Flow in Arteries

Coupled to CFD, the computation of FFR from CTA requires methods to extract models from image data and to incorporate boundary conditions that demonstrate the effect of the microcirculation (28,29). One contemporary development in image-based modeling of blood flow enables modeling of pulsatile coronary flow and pressure in realistic patient-specific models (18). Figure 4 depicts steps in the creation of an anatomic model of the coronary lumen from CTA data. During the model construction process, image segmentation algorithms extract the luminal surface of the major vessels and branches, up to the limits imposed by the resolution of CTA. This segmentation process involves extracting the topology of the coronary artery tree; identifying, analyzing, and segmenting coronary plaques in each vessel; and extracting the luminal boundary. For the finite element method used in the FFR_{CTA} technology, a mesh is

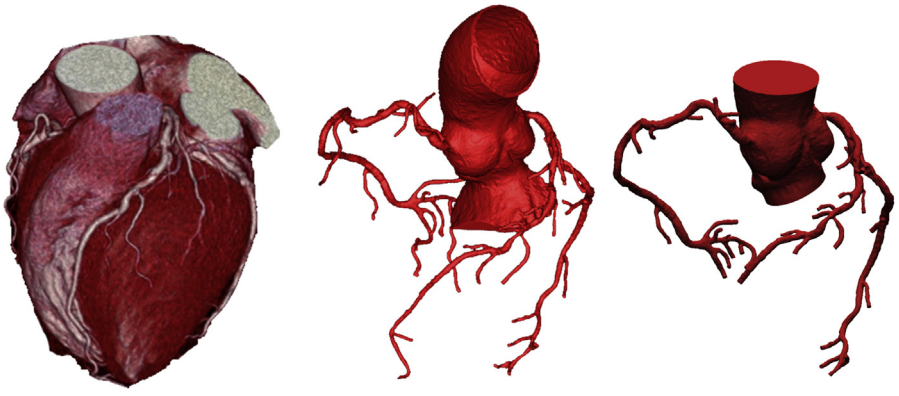

Figure 4 **Image Segmentation Steps for Computing FFR_{CTA}**

From **left**, volume-rendered image, lumen boundary surface segmented from image data, and final 3-dimensional model. Abbreviation as in Figure 1.

generated from the geometric model with millions of vertices and elements, and solved for velocity and pressure on a parallel supercomputer.

FFR Derived From CTA

Noninvasive computation of FFR requires coupling lumped parameter models of the heart, systemic circulation, and coronary microcirculation to a patient-specific model of the aortic root and epicardial coronary arteries extracted from CTA data. As shown in Figure 5, at the aortic inlet, a lumped parameter model representing the left ventricle is coupled to the aorta (18). At the aortic outlet, the model is used to enforce a relationship between pressure and flow (e.g., the aortic impedance). Notably, the cardiac output and the aortic pressure arise naturally through the interaction of the heart model and the model of the systemic circulation. For computation of FFR, parameters in the lumped models of the heart and systemic circulation are chosen so that the computed cardiac output matches that computed from an

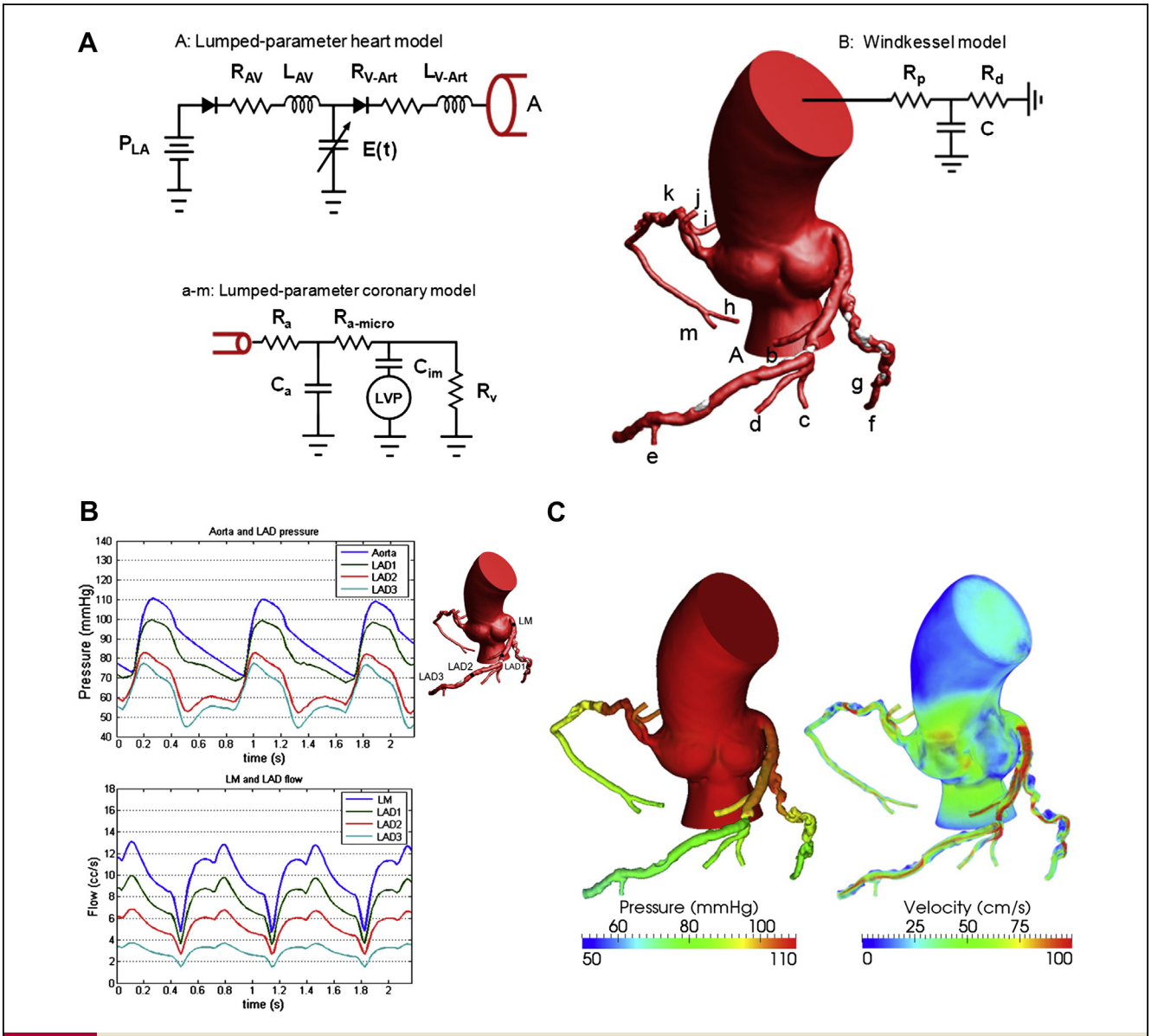

Figure 5 Mathematical Model for Pulsatile Coronary Flow

(A) Lumped parameter models are coupled to the aortic inlet and noncoronary vasculature and coronary microcirculation (18). *P* is the pressure, *R* the resistance, *C* the capacitance, *L* the inductance, and *E(t)* the elastance. Subscript *LA* is for the left atrium, *AV* for atrioventricular, *V-Art* for ventricle-arterial, *p* for proximal, *d* for distal, *a* for arterial, *im* for intermyocardial, and *V* for venous. **(B)** Pulsatile pressure and flow rate waveforms demonstrate reduced coronary flow in early systole due to contraction of the ventricle followed by increased flow in diastole resulting from relaxation of the ventricle. **(C)** Three-dimensional pressure and velocity fields are computed throughout the cardiac cycle. Note the pressure gradients and high-velocity jets across stenoses in the LAD, LCx, and right coronary artery (RCA). Abbreviations as in Figure 1.

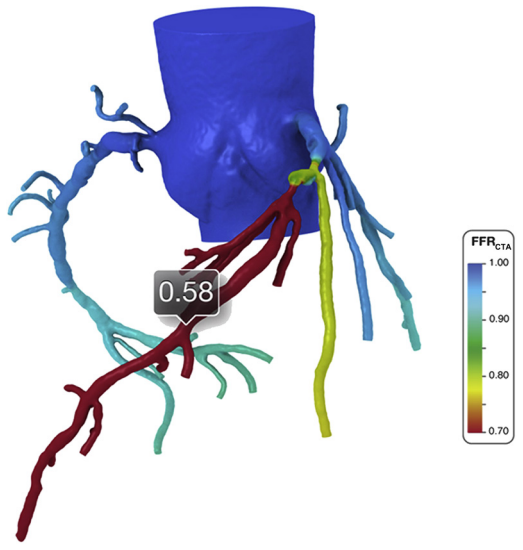

Figure 6 **FFR$_{CTA}$ Result for Patient With Serial Lesions in the LAD**

Color contours provide data on the distribution of FFR$_{CTA}$ throughout the coronary tree, and numerical values can be obtained at any location. Abbreviations as in Figure 1.

allometric scaling law, and the computed mean aortic pressure matches the patient's measured mean brachial pressure. At the coronary outlets, a relationship between pressure and flow based on a model of the coronary microcirculation is enforced.

A key step in assignment of coronary outlet boundary conditions for computation of FFR$_{CTA}$ is the prescription of unique resistance values for each outlet, based on the morphometry laws relating form and function described previously. Specifically, total coronary flow under basal conditions is computed from the myocardial wall volume extracted from CTA. Next, total coronary resistance is calculated from total coronary flow, and the mean aortic pressure is estimated from the mean brachial artery pressure. The basal resistance of each individual coronary outlet boundary is then computed by using total coronary resistance and a morphometry law of the form $R \propto d^{-k}$, inversely relating the resistance to flow of each branch to vessel diameter. Finally, for the lateral surface boundaries, a zero velocity (i.e., a "no-slip condition" for viscous fluids) is applied.

The final step in assigning boundary conditions is simulating maximum hyperemia by modeling the effect of adenosine on reducing the peripheral resistance of the coronary microcirculation downstream of the epicardial arteries extracted from CTA. Wilson et al. (30) showed that for arteries with normal CFR, in which the epicardial resistance would be expected to be small both at rest and during hyperemia, total coronary resistance at maximum hyperemia fell to 0.24 of the resting value with intravenous administration of adenosine 140 μg/kg/min. This dose underlies that which is administered for pharmacological stress testing and is the dose used for measurement of FFR. This change in resistance of normal coronary arteries provides an upper bound on the maximal change that can be achieved in patients with microcirculatory dysfunction and

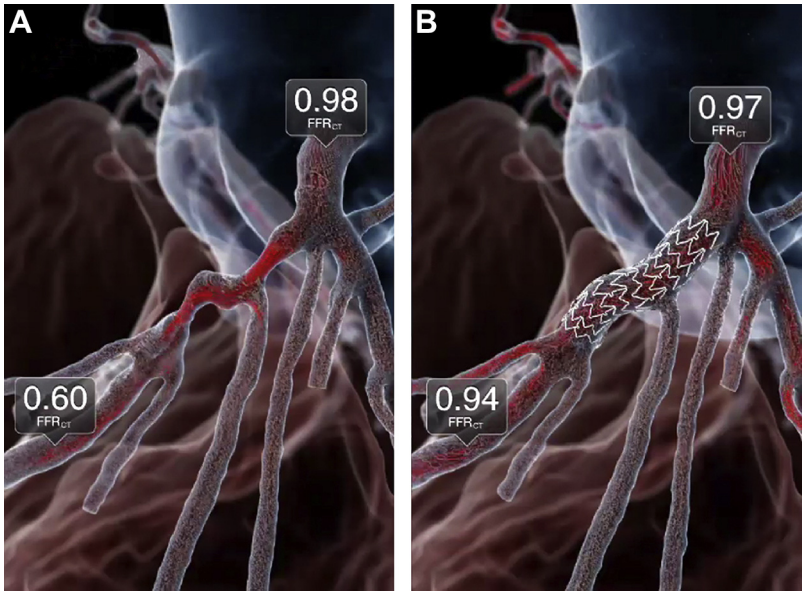

Figure 7 **Comparison of FFR$_{CTA}$ Results Before and After Simulated PCI With Stent Implantation**

(A) Before and **(B)** after percutaneous coronary intervention (PCI). FFR$_{CTA}$ values are superposed on images of particle trajectories. Abbreviation as in Figure 1.

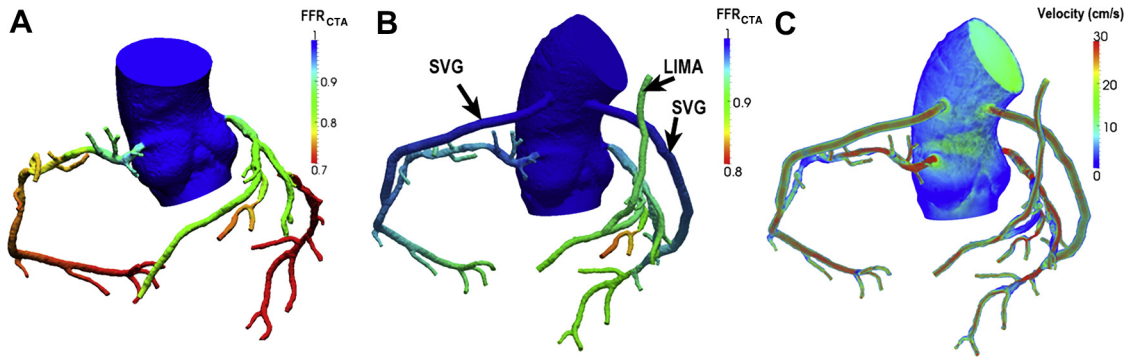

Figure 8 **Application of FFR$_{CTA}$ Technology to Predict Hemodynamic Changes Due to CABG**

(A) Pre-intervention FFR$_{CTA}$ demonstrates significant disease in RCA and LCx, including left main artery and RCA ostial lesions. **(B)** Post-coronary artery bypass graft (CABG) FFR$_{CTA}$ demonstrates marked reduction in vessel ischemia resulting from saphenous vein grafts (SVG) but little change in the LAD from the left internal mammary artery (LIMA). **(C)** Time-averaged blood velocity is shown in native vessels and bypass grafts. Abbreviations as in Figures 1 and 5.

represents an assumption made with invasive FFR, wherein the hyperemic microcirculatory resistance distal to a stenosis is assumed to be the same as that in the hypothetical case that the coronary arteries have no disease (31).

Upon generation of a discrete model (e.g., finite element mesh) of the ascending aorta and epicardial coronary arteries, and the definition of the boundary conditions for rest and hyperemic conditions, FFR$_{CTA}$ can then be determined by solving the equations of blood flow for the velocity and pressure fields. FFR$_{CTA}$ is then obtained by normalizing the mean hyperemic pressure field by the average mean hyperemic pressure in the aorta. The end result is a complete spatial distribution of FFR$_{CTA}$, as shown in Figure 6 for a patient with significant ischemia resulting from serial lesions in the left anterior descending coronary artery.

Limitations

Numerous artifacts may affect CTA interpretability, including calcification, motion, and misregistration. Because FFR$_{CTA}$ requires accurate anatomic models, these artifacts may limit accuracy. Thus, adherence to protocols that ensure good quality data and facilitate accurate lumen boundary descriptions is essential (32). Additional limitations of FFR$_{CTA}$ relate to assumptions in the physiological models that include population-specific as well as patient-specific data. Relationships relating myocardial mass to total coronary flow, the relative coronary microvascular resistance based on vessel size, or reductions in resistance in response to adenosine-mediated hyperemia will vary among patients. In patients with microvascular disease, models of adenosine-mediated hyperemia may overestimate the degree of vasodilation, resulting in FFR$_{CTA}$ values below those of measured FFR. Finally, no published data exist for FFR$_{CTA}$ in the evaluation of in-stent restenosis or for coronary artery bypass grafts.

Future Possibilities

CFD methods applied to CTA data have enabled noninvasive assessment of lesion-specific ischemia by FFR$_{CTA}$. Importantly, these methods may also enable prediction of changes in coronary flow and pressure from therapeutic interventions (e.g., percutaneous coronary intervention, coronary artery bypass graft) as shown in Figures 7 and 8. FFR$_{CTA}$ enables study of other hemodynamic metrics (e.g., CFR, shear stress, total plaque force). For example, computed blood velocity, as shown in Figure 8C, may allow evaluation of flow stagnation in bypass grafts. In addition, other physiological states such as graded exercise conditions can be modeled. Finally, the technology underlying FFR$_{CTA}$ is applicable to other common cardiovascular conditions, including peripheral, cerebrovascular, and renovascular disease, and may be used to determine whether vascular stenoses are hemodynamically significant as well as the relative benefit of therapeutic interventions.

Reprint requests and correspondence: Dr. James K. Min, Cedars-Sinai Medical Center, Cardiology, The Heart Institute, 8700 Beverly Boulevard, Taper Building, Room 1253, Los Angeles, California 90048. E-mail: james.min@cshs.org.

REFERENCES

1. Lucas FL, Siewers AE, Malenka DJ, Wennberg DE. Diagnostic-therapeutic cascade revisited: coronary angiography, coronary artery bypass graft surgery, and percutaneous coronary intervention in the modern era. Circulation 2008;118:2797–802.
2. Gould KL, Lipscomb K, Hamilton GW. Physiologic basis for assessing critical coronary stenosis. Instantaneous flow response and regional distribution during coronary hyperemia as measures of coronary flow reserve. Am J Cardiol 1974;33:87–94.
3. Uren NG, Melin JA, De Bruyne B, Wijns W, Baudhuin T, Camici PG. Relation between myocardial blood flow and the severity of coronary-artery stenosis. N Engl J Med 1994;330:1782–8.

4. Tonino PA, Fearon WF, De Bruyne B, et al. Angiographic versus functional severity of coronary artery stenoses in the FAME study: Fractional Flow Reserve Versus Angiography in Multivessel Evaluation. J Am Coll Cardiol 2010;55:2816–21.
5. Shaw LJ, Berman DS, Maron DJ, et al. Optimal medical therapy with or without percutaneous coronary intervention to reduce ischemic burden: results from the Clinical Outcomes Utilizing Revascularization and Aggressive Drug Evaluation (COURAGE) trial nuclear substudy. Circulation 2008;117:1283–91.
6. Pijls NH, De Bruyne B, Peels K, et al. Measurement of fractional flow reserve to assess the functional severity of coronary-artery stenoses. N Engl J Med 1996;334:1703–8.
7. Pijls NH, van Schaardenburgh P, Manoharan G, et al. Percutaneous coronary intervention of functionally nonsignificant stenosis: 5-year follow-up of the DEFER Study. J Am Coll Cardiol 2007;49:2105–11.
8. Tonino PA, De Bruyne B, Pijls NH, et al. Fractional flow reserve versus angiography for guiding percutaneous coronary intervention. N Engl J Med 2009;360:213–24.
9. Fearon WF, Bornschein B, Tonino PA, et al. Economic evaluation of fractional flow reserve-guided percutaneous coronary intervention in patients with multivessel disease. Circulation 2010;122:2545–50.
10. De Bruyne B, Pijls NH, Kalesan B, et al. Fractional flow reserve-guided PCI versus medical therapy in stable coronary disease. N Engl J Med 2012;367:991–1001.
11. Achenbach S, Daniel WG. Noninvasive coronary angiography—an acceptable alternative? N Engl J Med 2001;345:1909–10.
12. Budoff MJ, Dowe D, Jollis JG, et al. Diagnostic performance of 64-multidetector row coronary computed tomographic angiography for evaluation of coronary artery stenosis in individuals without known coronary artery disease: results from the prospective multicenter ACCURACY (Assessment by Coronary Computed Tomographic Angiography of Individuals Undergoing Invasive Coronary Angiography) trial. J Am Coll Cardiol 2008;52:1724–32.
13. Min JK, Shaw LJ, Berman DS. The present state of coronary computed tomography angiography: a process in evolution. J Am Coll Cardiol 2010;55:957–65.
14. Goldstein JA, Gallagher MJ, O'Neill WW, Ross MA, O'Neil BJ, Raff GL. A randomized controlled trial of multi-slice coronary computed tomography for evaluation of acute chest pain. J Am Coll Cardiol 2007;49:863–71.
15. Meijboom WB, Van Mieghem CA, van Pelt N, et al. Comprehensive assessment of coronary artery stenoses: computed tomography coronary angiography versus conventional coronary angiography and correlation with fractional flow reserve in patients with stable angina. J Am Coll Cardiol 2008;52:636–43.
16. Nissen SE. Limitations of computed tomography coronary angiography. J Am Coll Cardiol 2008;52:2145–7.
17. Melikian N, De Bondt P, Tonino P, et al. Fractional flow reserve and myocardial perfusion imaging in patients with angiographic multivessel coronary artery disease. J Am Coll Cardiol Intv 2010;3:307–14.
18. Kim HJ, Vignon-Clementel IE, Coogan JS, Figueroa CA, Jansen KE, Taylor CA. Patient-specific modeling of blood flow and pressure in human coronary arteries. Ann Biomed Eng 2010;38:3195–209.
19. Koo BK, Erglis A, Doh JH, et al. Diagnosis of ischemia-causing coronary stenoses by noninvasive fractional flow reserve computed from coronary computed tomographic angiograms. Results from the prospective multicenter DISCOVER-FLOW (Diagnosis of Ischemia-Causing Stenoses Obtained Via Noninvasive Fractional Flow Reserve) study. J Am Coll Cardiol 2011;58:1989–97.
20. Min JK, Leipsic J, Pencina MJ, et al. Diagnostic accuracy of fractional flow reserve from anatomic CT angiography. JAMA 2012;308:1237–45.
21. LaBarbera M. Principles of design of fluid transport systems in zoology. Science 1990;249:992–1000.
22. West GB, Brown JH, Enquist BJ. A general model for the origin of allometric scaling laws in biology. Science 1997;276:122–6.
23. Choy JS, Kassab GS. Scaling of myocardial mass to flow and morphometry of coronary arteries. J Appl Physiol 2008;104:1281–6.
24. Murray CD. The physiological principle of minimum work: I. The vascular system and the cost of blood volume. Proc Natl Acad Sci U S A 1926;12:207–14.
25. Kamiya A, Togawa T. Adaptive regulation of wall shear stress to flow change in the canine carotid artery. Am J Physiol 1980;239:H14–21.
26. Zarins CK, Zatina MA, Giddens DP, Ku DN, Glagov S. Shear stress regulation of artery lumen diameter in experimental atherogenesis. J Vasc Surg 1987;5:413–20.
27. Glagov S, Weisenberg E, Zarins CK, Stankunavicius R, Kolettis GJ. Compensatory enlargement of human atherosclerotic coronary arteries. N Engl J Med 1987;316:1371–5.
28. Taylor CA, Figueroa CA. Patient-specific modeling of cardiovascular mechanics. Annu Rev Biomed Eng 2009;11:109–34.
29. Taylor CA, Steinman DA. Image-based modeling of blood flow and vessel wall dynamics: applications, methods and future directions. Ann Biomed Eng 2010;38:1188–203.
30. Wilson RF, Wyche K, Christensen BV, Zimmer S, Laxson DD. Effects of adenosine on human coronary arterial circulation. Circulation 1990;82:1595–606.
31. Pijls NH, van Son JA, Kirkeeide RL, De Bruyne B, Gould KL. Experimental basis of determining maximum coronary, myocardial, and collateral blood flow by pressure measurements for assessing functional stenosis severity before and after percutaneous transluminal coronary angioplasty. Circulation 1993;87:1354–67.
32. Abbara S, Arbab-Zadeh A, Callister TQ, et al. SCCT guidelines for performance of coronary computed tomographic angiography: a report of the Society of Cardiovascular Computed Tomography Guidelines Committee. J Cardiovasc Comput Tomogr 2009;3:190–204.

Key Words: computational fluid dynamics ■ computed tomography ■ coronary artery disease ■ fractional flow reserve.